JPL RELEASE 43 P.

IN-8877

C/S MI700802

IN SITU MEASUREMENTS OF THE PLASMA BULK VELOCITY NEAR THE IO FLUX TUBE

(NASA-CR-176810) IN SITU MEASUREMENTS OF THE PLASMA BULK VELOCITY NEAR THE IO FLUX TUBE (Massachusetts Inst. of Tech.) 43 p HC A03/MF A01 CSCL 20I

N86-27075

Unclas G3/75 43457

BY

ALAN BARNETT

CENTER FOR SPACE RESEARCH
MASSACHUSETTS INSTITUTE OF TECHNOLOGY
CAMBRIDGE, MA 02139

OCTOBER, 1985

CSR-P-85-6 - J.G.R.

In situ Measurements of the Plasma Bulk Velocity Near the Io Flux Tube

by

Alan Barnett

Massachusetts Institute of Technology, Cambridge, Massachusetts

Abstract

We study the flow around the Io flux tube by analyzing the eleven spectra taken by the Voyager 1 Plasma Science (PLS) experiment in its vicinity. We determine the bulk plasma parameters using a procedure that uses the full response function of the instrument and the data in all four PLS sensors. The mass density of the plasma in the vicinity of Io is found to be 22,500±2,500 amu/cm^3 and its electron density is found to be 1500±200 cm^{-3}. We determine the Alfven speed using three independent methods; the values obtained are consistent and taken together yield V_A = 300±50 km/sec, corresponding to an Alfven Mach number of 0.19±0.02. For the flow pattern, we find good agreement with the model of Neubauer (1980), and conclude that the plasma flows around the flux tube with a pattern similar to the flow of an incompressible fluid around a long cylindrical obstacle of radius 1.26±0.1 R_{Io}.

1. Introduction

The Jovian satellite Io has been an object of great interest since the discovery that the intensity of the Jovian decametric radio emmission is strongly correlated with the phase angle of the satellite (Bigg, 1964). Much theoretical work has been done attempting to explain the correlation (for a review, see Goldstein and Goertz, 1983). When Voyager 1 flew within 20,000 km of Io on 5 March 1979, its field and particle experiments took data which have been used to test the theories of the interaction between Io and the Jovian magnetosphere.

The idea that a pair of Alfven wings forms attached to a conducting body when that body moves through a magnetized plasma is due to Drell et al (1965). Neubauer (1980) found that an exact solution of the nonlinear MHD equations can be used to describe in detail the magnetic, electric, and velocity fields in the vicinity of Io's Alfven wing. Analysis by Acuna et al (1981) showed that the Voyager magnetometer data are consistent with this theory. An indication in the data from the Voyager Plasma Science Experiment (PLS) that the predicted velocity perturbation is present has been noted by Belcher et al (1981).

Using the full response function of the instrument, we have analyzed the data taken by the PLS instrument during the Io flyby to determine the bulk plasma velocity, and our results confirm the existence of the Alfven wing. The data analysis consists of two distinct steps. First, the individual spectra must be analyzed in order to determine the plasma bulk velocity at the time of each spectrum taken during the Io flyby. Then the measured velocities must be compared to the flow pattern of a model of the Io-magnetosphere interaction.

In Section 2 of this paper, we describe the orbit and orientation of the spacecraft during the Io flyby. That section also contains a brief description of the PLS instrument. The precedure used to determine the plasma bulk velocity from the measured spectra is described in Section 3. The line dipole model of the flow around the flux tube is briefly described in Section 4. We have interpreted the velocities determined in Section 3 by comparing them to this model. The flow velocity measurements, supplemented only by the direction of the background (unperturbed) magnetic field, are sufficient to determine all of the parameters of the model. This determination is described in Section 5.

Since the flow perturbation and the magnetic field perturbation are linearly related, one can, in addition to the analysis described above, obtain values for the background flow velocity and the Alfven speed from a linear regression of the velocity data to the magnetic field data. The results of this analysis are stated in Section 6. The results of the preceding sections are summarized and conclusions are stated in Section 7.

2. The PLS Instrument and the Io Flyby

In this section we briefly describe the instrument and its orientation during the Io flyby. The Voyager Plasma Science Experiment consists of four modulated grid Faraday cups. A sketch of the instrument is shown in Figure 1. Three of the cups, called the A-cup, B-cup, and C-cup, comprise the main sensor. These three cups have the same pentagonal shape and are arrayed with their cup normals 20° from an axis of symmetry. The fourth cup, called the side sensor or D-cup, has a circular aperture. The normal to the D-cup aperture points in a direction 88° from the main sensor symmetry axis.

The Voyager spacecraft is three axis stabilized. The outward pointing symmetry axis of the PLS main sensor is parallel to the axis of the spaccecraft main antenna, which is pointed at the Earth during most of the mission. The D-cup is oriented such that it looked into corotating flow during the inbound pass of the Jupiter flyby.

On 5 March 1979, Voyager I flew through the inner magnetosphere of Jupiter. Its orbit is shown in Figures 2, 3a, and 3b. Figure 2 shows the projection of the spacecraft trajectory into the Jovian equatorial plane, in addition to the orientation of the main sensor symmetry axis (labeled S) and the D-cup normal (labeled D). The angles between the Jovian equatorial plane and the D-cup look direction and between the Jovian equatorial plane and the main sensor symmetry axis were 6° and 1°, respectively. As can be seen from this figure, the D-cup was looking into the co-rotating plasma throughout the inbound pass. As the spacecraft approached perijove, the corotating flow swung around towards the main sensor, almost coming down the symmetry axis near closest approach. As the spacecraft receded from

Jupiter, the flow direction shifted away from all of the cups. Several hours after the Io flyby, the spacecraft rolled about the symmetry axis, bringing the D-cup look direction closer to the co-rotating flow during much of the rest of the outbound pass. The closest approach to Io occurred on the outbound pass at about spacecraft event time (SCET) 1510. At that time, the direction of the bulk velocity of a rigidly corotating plasma would have been almost perpendicular to the main sensor symmetry axis.

Figures 3a and 3b are closeups of the Io flyby. The coordinate system used is a cartesian system (x,y,z) whose origin is the center of Io. The z-axis is parallel to the spin axis of Jupiter; the y-axis points from the center of Io to the center of Jupiter, and the x-axis, which points in the direction of rigid corotation, completes the right-handed orthogonal system. Fig. 3a is a projection of the orbit into the x-y plane, while Fig. 3b is a plot of the distance from the origin of that projection against the height above the plane. All distances are in units of the radius of Io.

The Io flyby occurred on the spacecraft's outbound pass, when Voyager I flew about 20 thousand kilometers due south of the satellite. Analysis of the magnetic field data (Acuna et al, 1981) showed that the spacecraft had passed several thousand kilometers upstream of the Alfven wing. Preliminary examination of the plasma data (Belcher et al, 1981) revealed a signature which was interpreted as being due to the velocity perturbation associated with the plasma flow around the flux tube. The approximate position of the intersection of the flux tube with the plane $z=-11.5R_{Io}$, based on the direction of the background magnetic field measured by Acuna et al, a rigidly corotating plasma, and an Alfven angle (defined in section 4) of 0.19 (the result obtained in the analysis described in Section 5), is also shown in Fig. 3a.

3. Analysis of the Spectra

During the Jupiter encounter, the PLS experiment took one complete high resolution (M-mode) spectrum every 192 seconds. The data which we have analyzed consist of the eleven spectra, taken between SCET 1451 and SCET 1523, which contain the velocity perturbation. The measurement of an entire M-mode spectrum takes 32 seconds to complete, and the SCETs quoted in the text are the hour and minute of the start time of the measurement. The spectra consist of 128 contiguous channels which span the energy-per-charge range of 10-5950 eV with a nomimal energy resolution of 3%. The position of the spacecraft at the start time of each spectrum is indictated by the tick marks on the trajectory plots of Figs. 3a and 3b.

During the Io flyby, the flow direction of a rigidly corotating plasma would have been almost perpendicular to the main sensor symmetry axis. Due to the large angle between the plasma bulk velocity and the look directions of the cups, accurate knowledge of the response function of the cups is required in order to analyze the data. The response function of the cups was derived by studying particle trajectories inside the cup. The resulting expression was tested by analyzing data taken during a cruise maneuver, when the spacecraft rotated such that the main sensor symmetry axis no longer pointed at the earth. Using the solar wind (with a sonic Mach number of about 20) as a test beam, the theoretical response function was found to be accurate to within a few percent for all angles of incidence (Barnett and Olbert, 1985).

Knowledge of the response function permits us to compute the current in each channel of each cup for a given plasma distibution function.

Inverting this procedure to find the distribution function from the currents is a more difficult task. We have solved this problem by parameterizing the distribution function and using a nonlinear least square fit routine to find the optimum values of the parameters.

The criterion used to define the "best fit" is the minimization of x^2, defined by

$$x^2 = \sum_i (D_i - A_i)^2 \qquad (1),$$

with respect to the plasma parameters. In Eq. (1), each of the D_i's is the measured "reduced distributions functions", defined below, and the A_i's are the corresponding simulated quantities which depend upon the plasma parameters. The solution to the extremum problem is found using a gradient search algorithm similar to that described in Bevington (1969).

Figures 4 and 5 are log-log plots of the "reduced distribution function" versus the equivalent proton velocity in each cup for the spectra taken at SCET 1500 and 1504. The "reduced distribution function" F and the equivalent proton velocity v_p are defined by

$$F = I_k / Wd_k \qquad (2)$$

$$v_p = (2ed_k/m_p)^{1/2} \qquad (3)$$

where I_k is the measured current in the k-th channel, d_k is the threshold voltage of the k-th channel, $Wd_k = d_{k+1} - d_k$ is the voltage width of the k-th channel, and m_p is the proton mass. In the figures, the staircases are the data, and crosses are the "best fit " simulations. The smooth curves show the contributions of the individual ionic components to the "best fits". All of the main sensor spectra are smooth and almost featureless, with a single, broad peak. Furthermore, in each spectrum the peak in the A-cup is in a higher channel than the peaks in the B- and C- cups. Since the D-cup was

pointed almost 180° from the direction of corotating plasma flow at this time, its currents are lower than those of the main sensors by more than an order of magnitude, and all but the first 20 channels or so are noise. The B- and C-cup spectra also contain features which look like absorbtion lines. These features, called dropouts, are caused by interference with another experiment on board the spacecraft. The fits use data from channels 1 through 72 in the A-cup, 1 through 20 in the D-cup, and 1 through 56 in the B- and C-cups, with the exception of the channels affected by the interference. We chose which channels to include in the fits by considering both the noise level in the instrument and the limitations set by our use of convected maxwellians to describe the particle distribution functions.

To determine macroscopic plasma parameters from these spectra is a difficult proposition. Since the flow is oblique to all of the cup normals, the results depend critically upon the cup response function at large angles. In addition, the plasma contains many different kinds of ions (Bagenal and Sullivan, 1981) which are probably not in thermal equilibrium. In order to get any results at all, we have had to make some assumptions about the chemical composition and the distribution functions of the various ionic species. These assumptions are:

1. The plasma consists of the following 6 ionic species; H^+, O^+, O^{2+}, S^+, S^{2+}, and S^{3+}.

2. The densities of the S^+, S^{2+}, and S^{3+}, components are fixed at 150 cm^{-3}, 183 cm^{-3}, and 64 cm^{-3}, respectively (see below).

3. The species all have the same bulk velocity.

4. The distribution function which describes each of the species is a convected maxwellian.

5. The heavy ion species all have the same temperature, but the proton component has an independent temperature.

6. The presence of suprathermal tails in the true distribution functions can be compensated for by including a additional "mock" ionic species with a higher temperature. We have parameterized this "hot" component as if it were O^+.

Measurements made by Voyager 1 inbound (Bagenal and Sullivan, 1981) lead us to expect the plasma to consist primarily of various ionization states of oxygen and sulfur. The values of A/Z^* for O^{2+}, O^+, S^{3+}, S^{2+}, and S^+ are 8, 16, 10 2/3, 16, and 32, respectively. In addition, we have included a proton component, which is important in the low channels of all of the cups because of its large thermal speed.

Experience with the nonlinear least squares fit procedure leads us to try to reduce the number of fit parameters whenever possible. In particular, if one permits the densities of all of the species to vary as fit parameters, one finds that the "best fit" values for some of them are negative; a very unphysical result. To remedy this situation, we have arbitrarily chosen the three ionization states of sulphur to have fixed densities. The values that we have used were extrapolated from the data taken at the same L-shell on the inbound pass (Fran Bagenal, private communication 1985).

The assumption of a common bulk velocity for all of the species is the least likely of the four assumptions to be violated. In the MHD approximation, the "frozen in" law requires all species to have the same velocity perpendicular to $\vec{B}$, and there is no reason to expect differential streaming along $\vec{B}$, either.

The assumption that the distribution functions are maxwellian is more difficult to justify. Since the self-maxwellization times for the various

species (computed using the densities and temperatures determined by Bagenal and Sullivan, 1981) are comparable to or greater than the residence time in the torus (Richardson and Siscoe, 1983) we should consider the maxwellian form as no more than a convient parameterization of the distribution function. As long as the true distribution functions do not have multiple peaks, a maxwellian should be a reasonably good approximation to the true distribution function around the maximum. Unfortunately, the true distribution functions undoubtedly have suprathermal tails. We have included the contribution of the tails by the addition of a "hot" component of O^+, also described by a maxwellian, but with a higher temperature. One should bear in mind that the density and thermal speed of this hot component should not be taken too literally; it should rather be thought of merely as a way to parameterize the contribution of the suprathermal tails.

Our ultimate justification for the assumption of maxwellian distributions for each ion species is that it is a good representation of the true distribution function which enables us to greatly reduce the amount of computer time necessary to compute the simulated currents necessary for the least squares fit (Barnett, 1983). In fact, without that assumption, no analysis of the data is possible. Unfortunately, the fact that the angle between the plasma bulk velocity and the cup normals is large implies that most of the signal comes from particles not near the peak of the distribution function. The simulations indicate that the largest contribution comes from particles about one thermal speed away from the peak. We must conclude that our approximation of maxwellian distributions is a possible source of error.

Although there is no reason to expect all of the ionic species to have the same temperature (the time scale for equipartition among the various ion species is longer than the residence time in the torus), the merging of the

peaks in the spectra makes it impossible to fit the temperatures independently. Furthermore, in analyzing many spectra, including inbound spectra (which are much easier to analyze because of more favorable geometry) we find that the spectra are best fit by the present assumptions of common temperature of heavy ion "core" distributions, the inclusion of a "hot" component to mock up suprathermal tails, and an independent proton temperature. Our fits, therefore, have ten parameters; the three components of the common bulk velocity, four densities (H^+, O^{2+}, O^+, and O^+_{hot}), and three temperature parameters (for H^+, heavy ions, and O^+_{hot}).

The parameters derived from the fits of the eleven spectra taken during the Io flyby are given in Table 1. Each velocity listed in Table 1 is the "best fit" plasma bulk velocity in a frame of reference which rotates about the spin axis of Jupiter with the orbital period of Io. (Note that Io is at rest in that frame.) The components listed are the projections of the velocity onto the unit vectors (at the position of the spacecraft at the time the spectrum was taken) of a cylindrical polar coordinate system whose polar axis is also the spin axis of Jupiter. The component V_d of the bulk velocity of a rigidly co-rotating plasma at the spacecraft location at the time of each spectrum is given in the column which is labeled V_{CR}; the components V_r and V_z for such a plasma are, of course, zero.

At SCET 1451, the deviation from corotation was small. As the spacecraft proceeded toward the flux tube, V_d first decreased, then increased until it was greater than V_{CR} before finally decreasing again to close to the corotation speed at SCET 1523. During the same time interval, V_r remained small before increasing greatly around SCET 1507, and then decreasing back to zero. This is the expected behavior as the plasma slows down and is deflected around the Io Alfven wing (see section 4).

The thermal speed w is defined by

$$w = (2kT/m)^{1/2} \qquad (4)$$

where k is the Boltzmann constant, T is the absolute temperature, and m is the ion mass. The column labeled w_{cold} gives the thermal speed of the O^+ and O^{2+} components; the thermal speed of the S^+, S^{2+}, and S^{3+} components is equal to $w_{cold}/\sqrt{2}$. The thermal speeds do not vary much during the flyby.

Throughout the Io flyby, the electron density n_e (computed using the assumption of charge neutrality) remains roughly constant, except for a decrease in the last spectrum (1523). The decrease is probably caused by a density gradient in the ambient medium which is unrelated to the Io interaction. Our estimate of n_e is consistent with the value of 1.6×10^3 cm^{-3} obtained by the Planetary Radio Astronomy (PRA) experiment (Birmingham et al, 1981).

The local Alfven speed decreases more or less steadily during the flyby, an effect due primarily to the monotonic decrease in the background magnetic field strength from about 2000 nT at 1451 to about 1700 nT at 1523 (Acuna et al, 1981). The change in the mass density is less important, due to the weaker dependence of the Alfven speed on the density.

We have quoted the "best fit" parameters without error estimates because of the difficulty involved in estimating the uncertainties. We believe that the uncertainties in the determination of the macroscopic plasma parameters are much greater than the formal errors obtained in the fit procedure, which do not take into account the possible violation of our assumptions or imperfections in our approximation to the instrument response function. Due to the unfavorable geometry, the fits are very sensitive to the shapes of the tails of the distribution functions and to

the cup response function. In all of these spectra, the geometry is such that the flow is almost perpendicular to the symmetry axis of the main sensor with the A-cup look direction closest to the flow. At SCET 1504, for example, the angles between the corotation direction and the directions of the cup normals for the A, B, C, and D cups were 67^{o}, 95^{o}, 98^{o} and 171^{o}, respectively. Although we believe that our knowledge of the cup response is very accurate, the response function must still be considered as a possible source of error.

Error analysis is further complicated by the existence of large off-diagonal terms in the error matrix (see Bevington, 1969). By fitting the same spectra with slightly differing assumptions (such as changing the assumed values of the densities of the sulphur species), and considering uncertainties due to violation of our various assumptions, we estimate the uncertainty in the velocity components to be about 1.5 km/sec, the uncertainty in the electron density to be less than 20%, and the uncertainty in the Alfven speed estimates to be about 15%.

The uncertainties in the densities of the individual species are much greater than the uncertainties in the electron density or in the total mass density, and they might be as high as a factor of two or more. The decrease in the density of the hydrogen component, however, is real; since the signal in the low channels of the D-cup is almost all protons, one can make accurate estimates of the proton density. One must, however, be very careful in interpreting the meaning of the density of the "hot" component. Changes in n_{hot} and w_{hot} denote changes in the non-maxwellian tail of the distribution function.

4. The Flux Tube Model

In this section we discuss the model of the Io-magnetosphere interaction which we have used to interpret the velocities determined in the preceding section. Our model, based on the work of Neubauer (1980), is summarized below.

As Io moves through the magnetospheric plasma, it generates the pair of cylindrical Alfven wings, as shown in Figure 6. The axis of each wing is parallel to the outgoing Alfven characteristic, defined by

$$\vec{V}_A^{\pm} = \vec{V} \pm \vec{V}_A \tag{5}$$

where the Alfven velocity $\vec{V}_A$ is defined by

$$\vec{V}_A = \vec{B}/\sqrt{(4\pi\rho)} \tag{6}$$

On the surface of the wing, there is a surface charge distribution and a surface current distribution, shown schematically in Figure 6. The surface charge distribution is the source of a line dipole electric field outside of the wing, while the surface current distribution is the source of a similar magnetic field. This model is equivalent to dropping the higher order terms in the multipole expansion of the fields due to currents and charges inside the volume of the wing. The total electric or magnetic field in the rest frame of Io is taken to be the sum of the field due to the sources associated with the Alfven wing and a uniform background field.

We are primarily interested in the velocity field outside of the wing. The flow velocity is the sum of a uniform background flow and a velocity perturbation which is related to the magnetic field perturbation by the relation

$$\delta\vec{V} = -\delta\vec{B}/(4\pi\rho)^{1/2} \tag{7}$$

where $\delta\vec{V}$ is the velocity perturbation, $\delta\vec{B}$ is the magnetic field perturbation, and ρ is the plasma mass density.

Voyager 1 flew south of Io, in the region in which $\vec{V}_A^+$ is the outgoing characteristic. In that region, all field variables are constants along the $\vec{V}_A^+$ direction. We therefore define Alfven coordinates (X,Y,Z) as follows: the center of Io is taken to be the origin; the unit vector $\hat{Z}$ is antiparallel to the vector $\vec{V}_A^+$; the unit vector $\hat{Y}$ points in the direction of $\hat{Z} \times \vec{V}_0$, where $\vec{V}_0$ is the bulk flow velocity of the unperturbed plasma with respect to Io; and the unit vector $\hat{X}$ is equal to $\hat{Y} \times \hat{Z}$.

We now write explicitly the components of the velocity field in the Neubauer model. We assume that the line dipole moment has magnitude Q and that its direction makes an angle ψ_o with the negative X axis. In Alfven coordinates, the velocity components are

$$V_X = V_{oX} - Q \cos(2\phi-\psi_o)/R^2 \tag{8a}$$

$$V_Y = - Q \sin(2\phi-\psi_o)/R^2 \tag{8b}$$

$$V_Z = V_{oZ} + Q \tan(\theta_A) \cos(2\phi-\psi_o)/R^2 \tag{8c}$$

where $\phi = \tan^{-1}(y/x)$, $R^2 = (X^2 + Y^2)$, θ_A, called the Alfven angle, is the angle between $\vec{B}_o$ and $\vec{V}_A^+$, and Q is a parameter which describes the strength of the line dipole. If Io is a perfect conductor, Q can be expressed in terms of the background bulk speed V_0, the Alfven angle θ_A, the effective radius of Io R_c, the Alfven Mach number M_A $(=V_o/V_A)$, and θ, the complement of the angle between V_o and B_o, as

$$Q = V_o R_c^2 \cos\theta_A /(1 + M_A^2 + 2M_A \sin\theta)^{1/2} \tag{9}$$

The quantity R_c is the radius of a perfectly conducting sphere that would produce the given velocity perturbation. If the conductivity of Io is finite,

R_c would be less than R_{Io}. If the region of high conductivity is an extended ionosphere which surrounds Io, R_c may be greater than R_{Io}.

The angle ψ_o is related to the Hall term in the generalized Ohm's law for Io's ionosphere (Herbert and Lichtenstein, 1980). For the case $\psi_o=0$, (Hall currents negligible), the projection of the flow field into the X-Y plane is simply that of the potential flow of an incompressible fluid around an infinite cylinder.

In order to compare Eqs. 8a-8c with the experimental data, Alfven coordinates must be related to some coordinate system whose definition does not depend upon any measured quantity (the orientation of the Alfven coordinate system depends upon the direction of the vector $\vec{V}_A^+$, which in turn depends upon the background bulk velocity $\vec{V}$, which is not known a priori). To do this, we define "magnetic coordinates" (x_{mag}, y_{mag}, z_{mag}) as follows: the origin of the coordinate system is the center of Io; the unit vector $\hat{z}_{mag}$ is antiparallel to the direction of the extrapolated background magnetic field at the location of the spacecraft at SCET 1500, as quoted in Acuna et al (1981); the unit vector $\hat{x}_{mag}$ lies in the plane containing $\hat{z}_{mag}$ and the direction of strictly corotating flow, making an acute angle with the flow direction; and $\hat{y}_{mag}$ is defined so as to form a right-handed coordinate system. The components of the $\hat{z}_{mag}$ along the x-,y-,and z-axes of figures 3a and 3b are 0.1, -0.3, and 0.95, respectively. The relative orientation of the Alfven coordinate system and the magnetic coordinate system can be described by a sequence of two rotations (see Fig 7). First one rotates about $\hat{z}_{mag}$ by an angle α, then one rotates about $\hat{Y}$ by an angle $-\theta_A$.

Our model therefore has six free parameters which have to be determined from the data: V_{ox}, V_{oz} (V_{oy} is zero by definition), ψ_o, θ_A, and Q (the five parameters in Eqs. 4a, 4b, and 4c), plus the angle α. Since we have 33 data points (the three components of $\vec{V}$ for each of the eleven spectra), the system

is multiply overdetermined. One passing remark: note that θ_A enters twice; it appears in Eq. 4c, and it appears in the rotation matrix which defines the transformation between magnetic coordinates and Alfven coordinates.

The model just described is a solution of the MHD equations for the flow of a uniform plasma around a spherical conducting body. The solution is valid for the special case where the unperturbed plasma is spatially uniform, and there are no perturbations of the plasma density or pressure, or of the magnitude of the magnetic field.

For the case of the Io interaction, the unperturbed state is definitely non-uniform; effects due the curvature of the background magnetic field lines and of the background velocity streamlines might be important. As long as the scale length characteristic of gradients in the background quantities is large compared to the scale length characteristic of the perturbation, these effects should be small. A characteristic length for gradients in the background magnetic field and velocity field is the distance from Io to Jupiter, about six Jovian radii or 430,000 km. A length scale which characterizes the perturbation is the distance from Io of the spacecraft at the time that the perturbations were observed; about 18 Ionian radii or 33,000 km. The ratio of the scale lengths is ~0.08. We therefore expect the these gradients will effect the details, but not the overall picture, of the Io-magnetosphere interaction as observed by Voyager 1.

Potentially more serious are effects due to density and pressure gradients within the Io plasma torus; these gradients have a scale length of about 1 Jovian radius (72,000 km) (Bagenal and Sullivan, 1981). For example, the electron density determinations included in Table 1 vary by about 37%. The reader must keep these facts in mind when evaluating the fit to the model described in the next section.

5. Interpretation of the Measured Velocities

We used the bulk velocities given in Table 1 to obtain a "best fit" for the 6 quantities (V_{oX}, V_{oZ}, θ_A, α, ψ_o, and R_c) which describe our model of the flux tube. The results are given in Table 2. Comparison of the data with the theory is complicated by the curvature of the background flow. In particular, one has to correct for the increase in the speed of rigid corotation as the spacecraft recedes from Jupiter. As can be seen from Table 1, the corotation speed increases by 4 km/sec between the first and last spectra included in the fit. We compensated for this by correcting V_ϕ in the input data for each spectrum by an amount equal to the difference between the local corotation speed and the corotation speed at SCET 1500. The uncertainties quoted in Table 2 were obtained by repeating the fitting procedure with different methods of correcting for the curvature of the streamlines and for the changing corotation speed.

Figure 8 shows a plot of the projection of the "corrected" velocity $\vec{V}$ into the X-Y plane for all eleven spectra, where we have used the values of θ_A and α quoted in Table 2 to define the Alfven coordinate coordinate system. The tails of the arrows representing the velocity vectors are positioned at the location of the spacecraft at the time of the start of the corresponding measurement. Superimposed on the measured velocity vectors are the streamlines of the model flow. Figure 9 shows each of the three components of $\vec{V}$ as a function of time, along with a smooth curve which represents the line dipole flow model.

We now discuss the parameters listed in Table 2. The components of the background flow velocity $\vec{V}_o$ in the (x,y,z) coordinate system of Figures 3a and 3b are 0.8±1.5 km/sec, 57.3±1.5 km/sec, and -1.1±1.5 km/sec. We see that these values are consistent with rigid corotation (V_x=56.0 km/sec, V_y=V_z=0).

The angle ψ_o is consistent with zero, indicating that the Hall currents are not important.

The value of R_c of 2285±200 km or about 1.25 R_{Io} is consistent with the determination by Acuna et al, and it suggests that the region of large conductivity is Io's ionosphere.

The value of the Alfven angle θ_A is 0.19±0.02 radians, which is greater than the value of 0.15±0.01 obtained by Acuna et al. Using the formula

$$V_A = V_O \cos(\theta + \theta_A)/\sin \theta_A \qquad (10),$$

which is quite easily derived from the definition of θ_A and geometrical considerations, one obtains the value of 300±30 for V_A. Note that only the velocity data and the <u>direction</u> of the background magnetic field are required for this determination of V_A. Comparison with the values of V_A quoted in Table 1, obtained from local measurements of the mass density and magnetic field strength, show excellent agreement. This agreement is confirmation of the work of Drell et al (1965).

6. Comparison with the Magnetic Field Results

Up to now, we have not used the measured magnetic field perturbations in our analysis, although the model of the plasma flow around the Io flux tube which we have used predicts that each component of the velocity perturbation and the corresponding component of the magnetic field perturbation are related

by Equation (7). We now test this relation by assuming that $\delta\vec{V}$ and $\delta\vec{B}$ are related by the equations

$$\delta V_X = \alpha_X + \gamma_X \delta B_X \quad (11a)$$

$$\delta V_Y = \alpha_Y + \gamma_Y \delta B_Y \quad (11b)$$

$$\delta V_Z = \alpha_Z + \gamma_Z \delta B_Z \quad (11c)$$

where α_X, α_Y, α_Z, γ_X, γ_Y, and γ_Z are constants to be determined. The "best fit" values of the α's and the γ's were determined using the method of least squares, utilizing the magnetic field results of Acuna et al (1981). The results of the linear regression for each components are given in Table 3. Also given in Table 3 is the correlation coefficient r for each fit, and the Alfven speed derived from the results. The correlation coefficients are all close to -1, indicating that the corresponding components $\delta\vec{V}$ and $\delta\vec{B}$ are well anti-correlated, as predicted by the theory.

Figure 10 is a plot of the projection of $\delta\vec{V}$ and $\delta\vec{B}$ into the X-Y plane (Alfven coordinates) for the eleven analyzed M-mode spectra. As in Figure 9, the location of the tails of the vectors represents the position of the spacecraft at the time of the measurement.

To within the experimental uncertainty, the values obtained for the α_X, α_Y and α_Z are consistent with zero (implying rigid corotation). The values of γ_X, γ_Y and γ_Z should be the same for all three components; this value should be proportional to (plasma mass density)$^{-1/2}$. The values of γ_X and γ_Y agree to within 6%, while the value of γ_Z is about 25% higher. Since the Z-components of $\vec{B}$ and $\vec{V}$ are much smaller than the other components, while the uncertainty in the determination of all of the components is about the same, one expects the error in the determination of γ_Z to be much larger than the error in the determination of γ_X and γ_Y. In particular, none of the measured values of V_Z is greater than three times the uncertainty in its measurement.

We therefore conclude that our results are consistent. We can use the spread in the values of the γ_i to obtain an error estimate for V_A. We conclude from this line of reasoning that $V_A = 325 \pm 50$ km/sec. This value, obtained by completely independent information, agrees well with the result obtained using the local plasma density measurements (see Table 1) and the result inferred from the best fit to the flow model (see the discussion which follows Equation 10). The three determinations taken together yield $V_A = 300 \pm 50$ km/sec.

7. Summary and Conclusions

This work marks the first use of the knowledge of the full response function of the PLS instrument in analyzing data. The response of the instrument is known to within a few percent for all angles of incidence (Barnett and Olbert). A limitation is that this knowledge can only be of practical use when the distribution functions of the ion species can be well described by a convected maxwellian (or bimaxwellian). The inclusion in the analysis of the signals in all four cups is a great constraint, however. The fact that we are able to obtain excellent fits in all three cups of the main sensor, and reasonable fits to the side sensor (which looked almost antiparallel to the flow) indicates that our assumptions are not badly violated and illustrates the power of multi-sensor analysis.

Our results confirm the essentials of the Neubauer's (1980) model; the measured velocities can be understood as potential flow around a cylinder. The obstacle to the flow is not Io itself, however, but rather is the Alfven wing which is attached to Io. The Alfven wing is thus seen to be a very real object.

As is the case for the magnetic field measurements of Acuna et al (1981), we are unable to determine the conductivity of Io from our measurements, for we can only measure the dipole moment of the flow perturbation. Since the dipole moment which we infer is so large, we conclude that the electrical resistence of Io is comparable to or very much much less than the $\mu_o V_A$ (the characteristic impedence of the medium). Under the assumption that Io is a perfect conductor, we find the radius of the flux tube to be ~1.25 R_{Io}, implying that the region of high conductivity is the ionosphere of Io, rather than the satellite itself. For this case, the total current flowing through (or around) Io is given by (see Neubauer, 1980)

$$I = 4B_o R_c M_A / \mu_o \qquad (12)$$

Using the values of $M_A = 0.19$, $B_0 = 1.9 \times 10^{-6}$ Tesla, and $R_c = 2.3 \times 10^6$ m, we find the $I = 2.6 \times 10^6$ amps. These results all agree well with the conclusions drawn by Acuna et al (1981).

The one result which agrees less well with Acuna et al is the determination of the Alfven angle; our value of 0.19±0.02 radians is slightly greater than their value of 0.15±0.01 radians. Our direct in situ measurement of the plasma mass density and the results of the linear regression between the bulk velocity components and the corresponding magnetic field perturbation both imply a lower Alfven speed and hence a larger Alfven angle. One must bear in mind the fact that the Alfven speed is not constant over the entire region of interest, a fact which contradicts one of the assumptions made by Neubauer in his model of the Io-ionosphere interaction. This minor discrepency might be caused by effects due to gradients in the background plasma. When one considers the extent to which the unperturbed state of the plasma differs from the uniform background assumed by the theory, one concludes that the theory and experiment agree as well as can be expected.

8. Acknowledgements

I would like to thank John Belcher and Stan Olbert for their helpful suggestions, and Fran Bagenal for her help in extrapolating the inbound plasma data to facilitate the fits. I would also like to thank one of the referees for the thorough job he did. This work was sponsored in part by the National Aeronautics and Space Administration and performed under contract 953733 to the Massachusetts Institute of Technology from the Jet Propulsion Laboratory.

References

Acuna, M.H., F.M. Neubauer, and N.F. Ness; Standing Alfven Wave Current System at Io: Voyager I Observations. J. Geophys. Res 86, 8513, 1981

Bagenal, F. and J.D. Sullivan; Direct Plasma Measurements in the Io Torus and Inner Magnetosphere of Jupiter. J. Geophys. Res. 86, 8477, 1981

Barnett, A.S.; Analysis of Data from the Voyager Plasma Science Experiment Using the Full Cup Response. PhD thesis MIT 1983

Barnett, A.S.; The Response Function of the Voyager Plasma Science Experiment. NASA technical report CSR-TR-84-1 1984

Barnett, A.S., and S. Olbert; The Response Function of Modulated Grid Faraday Cup Plasma Instruments. Submitted to Reviews of Scientific Instruments 1984

Belcher, J.W., C.K. Goertz, J.D. Sullivan, and M.H. Acuna; Plasma Observations of the Alfven Wave Generated by Io. J. Geophys. Res. 86, 8508, 1981

Bevington, P.R.; Data Reduction and Error Analysis for the Physical Sciences. McGraw-Hill 1969

Bigg, E.K.; Influence of the Satellite Io on Jupiter's Decametric Emmission. Nature 203,1008, 1964

Birmingham, T.J., J.K. Alexander, M.D. Deutsch, R.F. Hubbard, and B.M. Pedersen; Observations of Electron Gyroharmonic Waves and the Structure of the Io Torus. J. Geophys. Res. 86, 8497, 1981

Bridge, H.S., J.W. Belcher, R.J. Butler, A.J. Lazarus, A.M. Mauretic, J.D. Sullivan, G.L. Siscoe, and V.M. Vasyliunas; The Plasma Experiment on the 1977 Voyager Mission. Space Sci. Rev. 21, 259, 1977

Drell, S.D.,H.M. Foley, and M.A. Ruderman; Drag and Propulsion in the Ionosphere. An Alfven Propulsion Engine in Space. J. Geophys. Rev. 70, 3131, 1965

Goldstein, M.L. and C.K. Goertz; Theories of Radio Emmision and Plasma Waves. Chapter 9 in Physics of the Jovian Magnetosphere, A.J. Dessler, editor. Cambridge University Press, 1983

Herbert, F. and B.R. Lichtenstein; Joule Heating of Io's Ionosphere by Unipolar Induction Currents. Icarus 44, 296, 1980

Neubauer, F.M.; Nonlinear Standing Alfven Wave Current System at Io: Theory. J. Geophys. Res. 85, 1171, 1980

Richardson, J.D., and G.L. Siscoe; The Non-maxwellian Energy Distribution of Ions in the Warm Io torus. J. Geophys. Res. 88, 8097, 1983

Table 1

Plasma Parameters Derived from PLS Spectra Taken Near Io

SCET	V_r	V_ϕ	V_z	n_{H+}	w_{H+}	n_{Hot}	w_{Hot}	n_{o++}	n_{o+}	w_{cold}	ρ_m	n_e	V_A	V_{CR}
1451:16	-0.3	55.2	0.1	44	82	295	46	61	247	28	2.24	1420	290	54.8
1454:28	-0.3	55.7	-0.1	50	75	344	42	55	216	25	2.26	1430	284	55.2
1457:40	-0.2	53.2	0.5	50	76	345	42	53	207	26	2.24	1420	282	55.6
1500:52	-0.2	50.7	0.7	63	84	316	43	65	193	27	2.20	1410	281	56.0
1504:04	9.4	47.0	-1.7	58	83	348	42	33	188	25	2.19	1370	277	56.4
1507:16	12.0	56.1	-5.5	37	94	271	44	101	292	27	2.17	1510	262	56.8
1510:28	1.2	64.7	-3.8	9	56	151	53	246	327	32	2.43	1690	253	57.2
1513:40	1.6	65.1	-2.5	22	64	272	42	117	228	28	2.26	1460	258	57.6
1516:52	-0.3	62.8	-1.8	21	60	214	46	108	284	29	2.24	1440	255	58.0
1520:04	0.0	60.8	-1.0	15	64	162	48	87	355	30	2.24	1410	251	58.4
1523:16	0.0	60.3	-0.1	16	48	157	48	72	329	29	2.16	1230	252	58.8

Speeds in km/sec

Number densities in cm^{-3}

Mass densities in 10^4 AMU/cm^3

Table 2

"Best Fit" Parameters for Incompressible Flow Model

V_X	V_Z	θ_A	α	ψ	R_c
57.0 ± 2.0	-6.2 ± 1.3	0.19 ± 0.02	0.02 ± 0.05	0.1 ± 0.1	1.26 ± 0.1

V_X, V_Z in km/sec, θ_A, α, ψ in radians, R_c in Ionian radii (R_{Io})

Table 3

Results of Linear Regression

$\delta V_x = 0.3 - .166\ \delta B_x$ $\quad r = -.99$

$\delta V_y = -0.9 - .157\ \delta B_y$ $\quad r = -.95$

$\delta V_z = -0.9 - .205\ \delta B_z$ $\quad r = -.94$

$V_A = 325 \pm 50$ km/sec

δV in km/sec

δB in nT

Figure Captions

Figure 1 The PLS instrument, consisting of four modulator grid Faraday cups. The D-cup look direction is 88° from the axis of symmetry of main sensor, which consists of the A-, B-, and C-cups. During the Io flyby, the flow direction of a rigidly corotating plasma was roughly anti-parallel to the look direction of the D-cup.

Figure 2 The Voyager 1 Jupiter encounter. The projection of the spacecraft trajectory into the Jovian equatorial plane is shown, along with the direction of the main sensor symmetry axis (S) and the D-cup look direction (D). The angle between S (D) and the Jovian equatorial plane during the encounter was 1° (6°), respectively. Also shown are the orbits of the Gallilean satellites (in order of increasing distance from Jupiter) Io, Europa, Ganymede, and Callisto. Note that during the Io flyby, which occured during the outbound pass, the flow direction of rigidly corotating plasma was roughly anti-parallel to the look direction of the D-cup, and almost perpendicular to the main sensor symmetry axis.

Figure 3 The Io flyby. The coordinate system used in these figures is defined as follows: the origin of the cartesian system is the center of Io; the z-axis is parallel to the spin axis of Jupiter; the y-axis points toward the center of Jupiter; and the x- axis points in the direction of rigidly corotating plasma flow. The circle labeled "Location of Io Flux Tube" is the intersection of the flux tube (using the orientation deduced from plasma measurements) with the plane $z=-11.5R_{Io}$.

Figure 4 Reduced distribution function versus equivalent proton speed for the spectrum taken at SCET 1500. The reduced distribution function is defined as the current in a given energy channel divided by the voltage width of that channel. The equivalent proton speed is related to the modulator voltage by $v_p = \sqrt{(2e\phi/m)}$, where v_p is the equivalent proton speed, e is the elementary charge, ϕ is the modulator voltage, and m is the proton mass. The "staircase" is the data, the crosses are the "best fit" simulation, and the smooth curves are the contributions of the individual species, as indicated.

Figure 5 Reduced distribution function versus equivalent proton speed for the spectrum taken at SCET 1504 (see the caption for Figure 4).

Figure 6 Io's Alfven Wings. Two views are shown of the Alfven wing and associated current system, Figure 6a shows the Alfven wings as seen looking along the flow direction of a rigidly corotating plasma. Figure 6b shows the Alfven wings as viewed by an observer located on the line which connects Jupiter and Io.

Figure 7 The relative orientation of the magnetic coordinate system and the Alfven coordinate system. To go from Magnetic to Alfven coordinates, rotate first about $\hat{z}_{mag}$ by an angle α, then about $\hat{Y}$ by an angle $-\theta_A$.

Figure 8 Plasma bulk velocity in the vicinity of Io. The dark arrows represent the projections of the bulk flow velocity into the X-Y plane (for the definition of the coordinate system, see the text or the caption to Figure 7). The tails of the arrows are located at the position of the spacecraft at the time that the measurement was taken. The dotted lines are the streamlines of the model flow.

Figure 9 Flow velocity versus time. The smooth curves are the "best fit" model velocities, while the data points are shown with error bars which correspond to an uncertainty of ± 1.25 km/sec.

Figure 10 Velocity and magnetic field perturbations during the Io flyby. The projection into the X-Y plane (Alfven coordinates) is shown. The solid arrows represent the velocity perturbations, and the broken arrows represent the magnetic field perturbation from Acuna et al. The tails of the arrows are located at the position of the spacecraft at the time of the measurement. The expected anti-correlation of the corresponding magnetic field and velocity perturbations is evident.

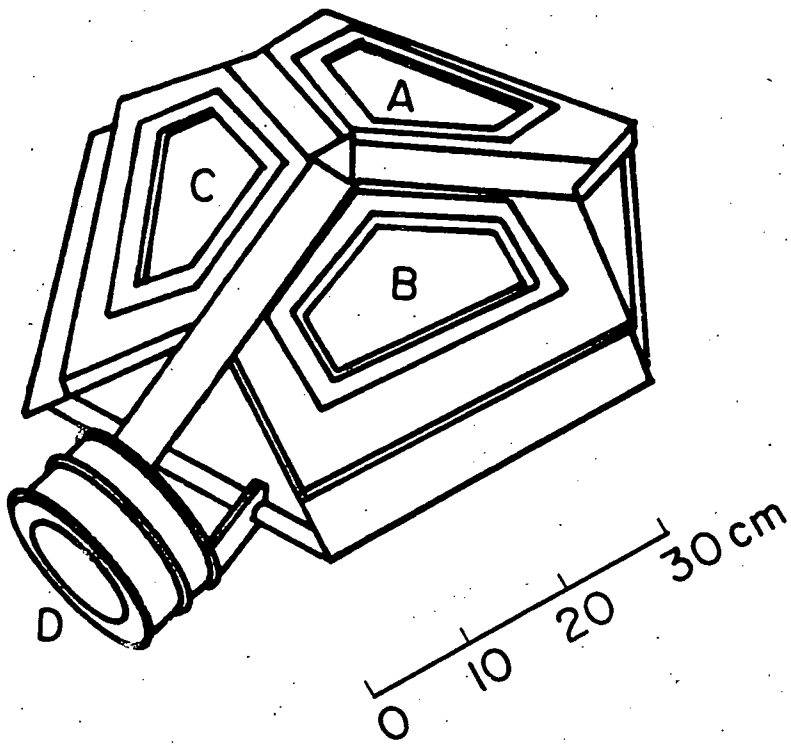

Figure 1

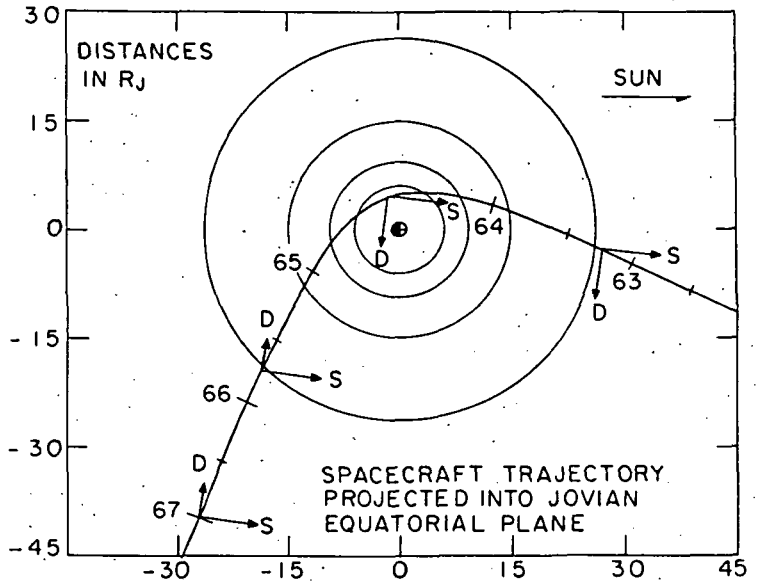
30
15
0
-15
-30
-45
-30
-15
0
15
30
45
DISTANCES
IN R_J
SUN
S
64
D
65
S
63
D
D
S
66
D
67
S
SPACECRAFT TRAJECTORY
PROJECTED INTO JOVIAN
EQUATORIAL PLANE

Figure 2

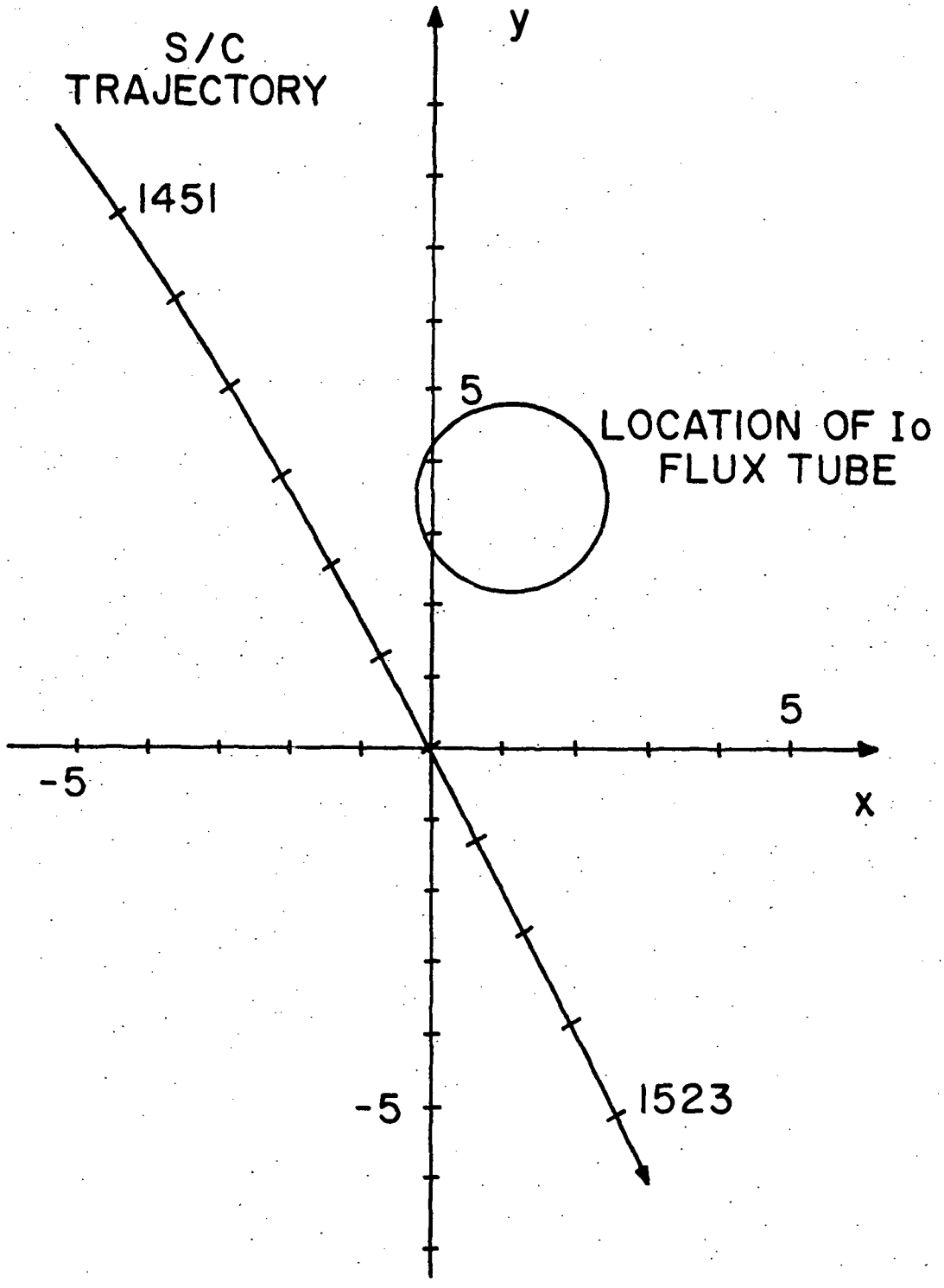

Figure 3a

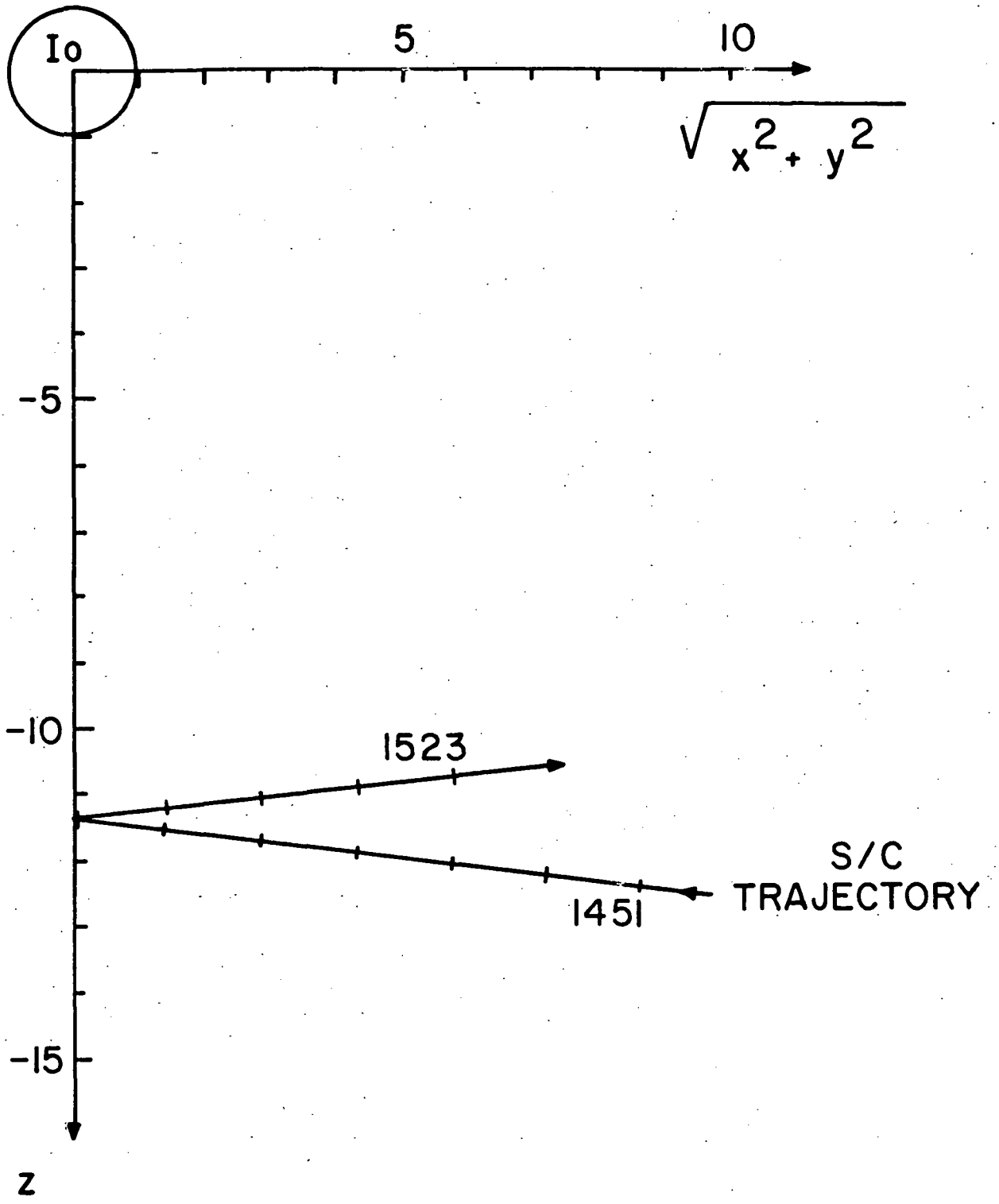

Figure 3b

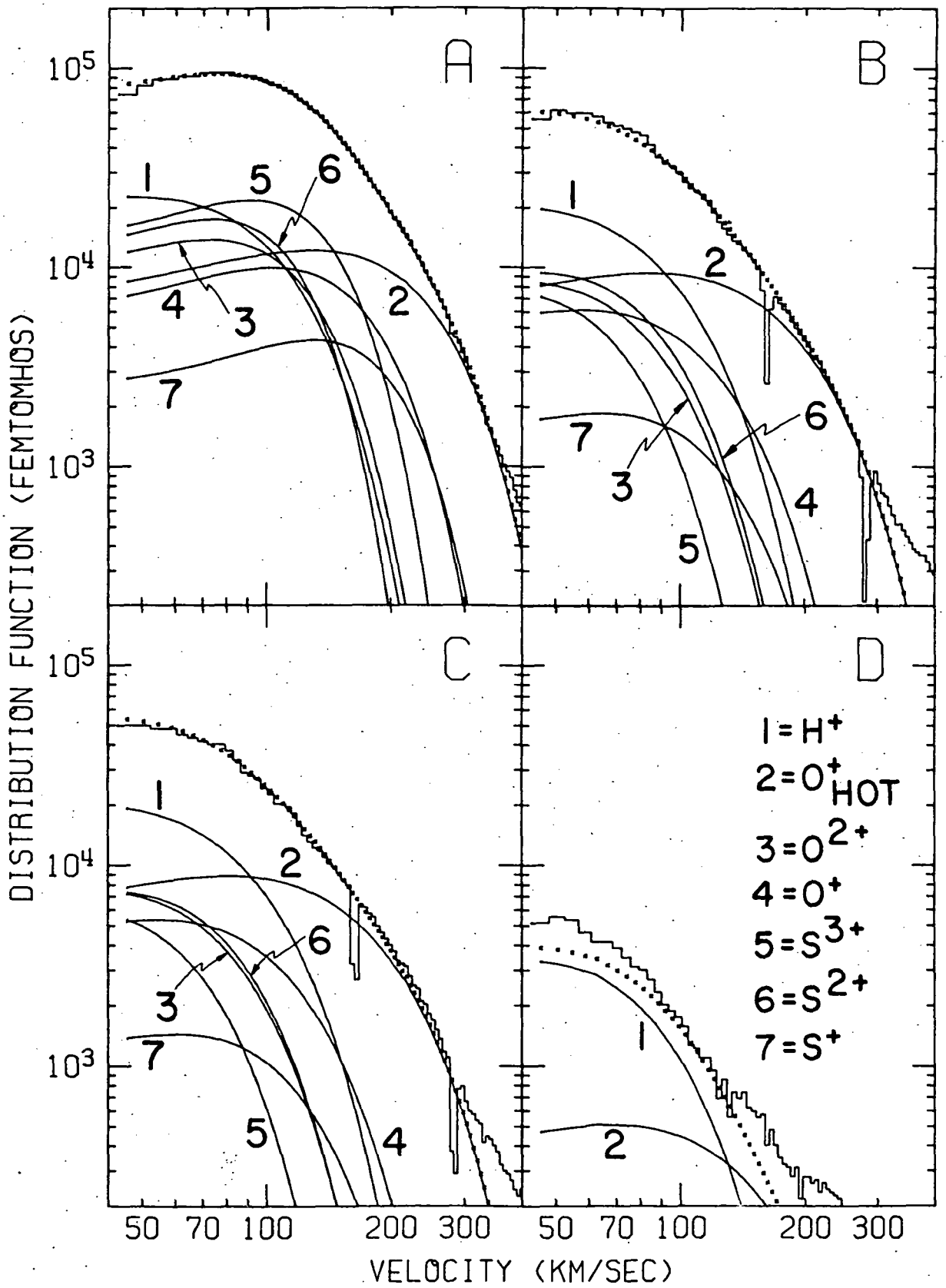
A
B
C
D
10^5
10^4
10^3
DISTRIBUTION FUNCTION (FEMTOMHOS)
1
2
3
4
5
6
7
50 70 100 200 300
VELOCITY (KM/SEC)
1=H+
2=O+HOT
3=O2+
4=O+
5=S3+
6=S2+
7=S+

Figure 4

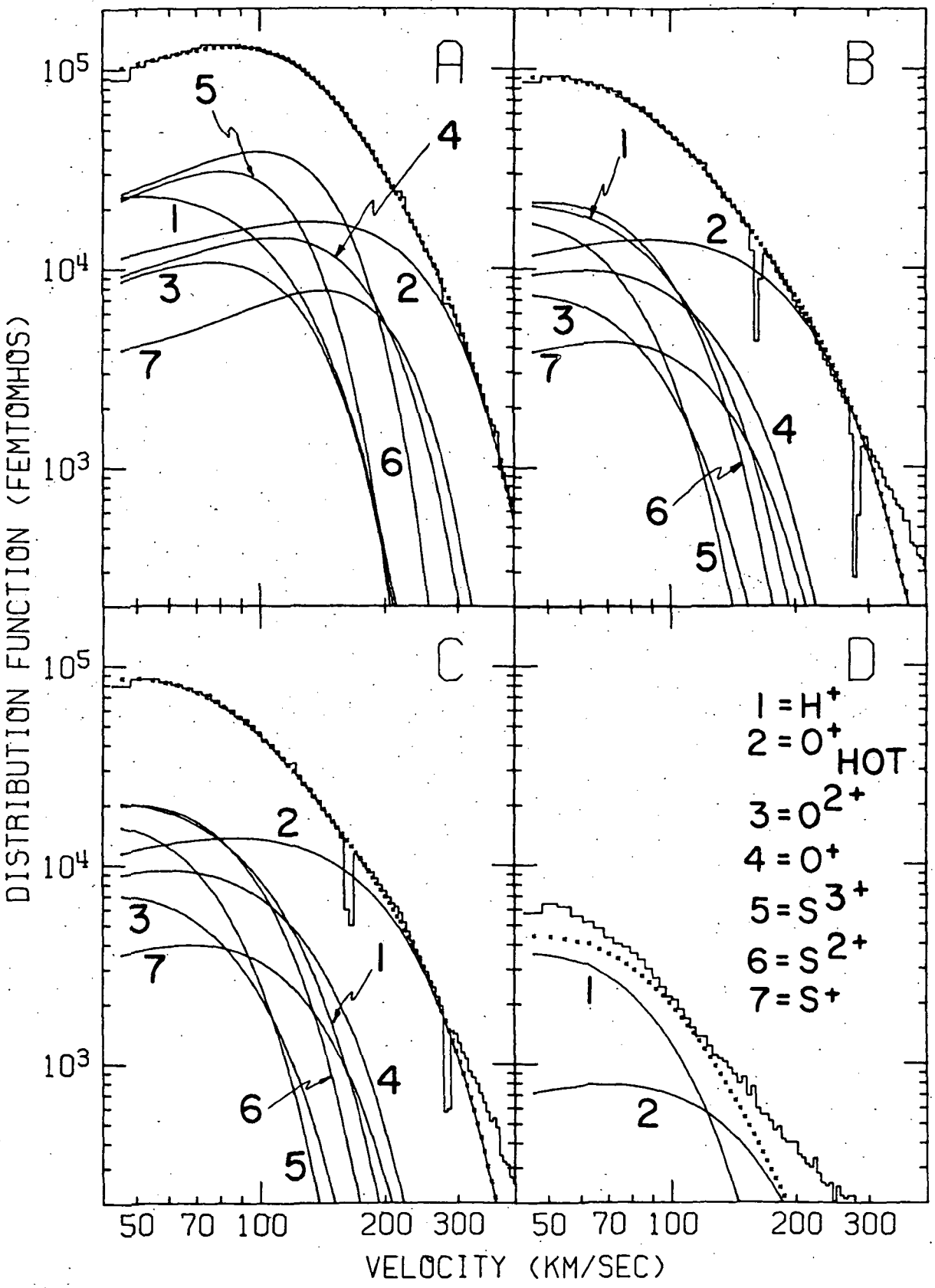
A
B
C
D
DISTRIBUTION FUNCTION (FEMTOMHOS)
VELOCITY (KM/SEC)
10^5
10^4
10^3
50 70 100 200 300
1 = H^+
2 = O^+ HOT
3 = O^{2+}
4 = O^+
5 = S^{3+}
6 = S^{2+}
7 = S^+

Figure 5

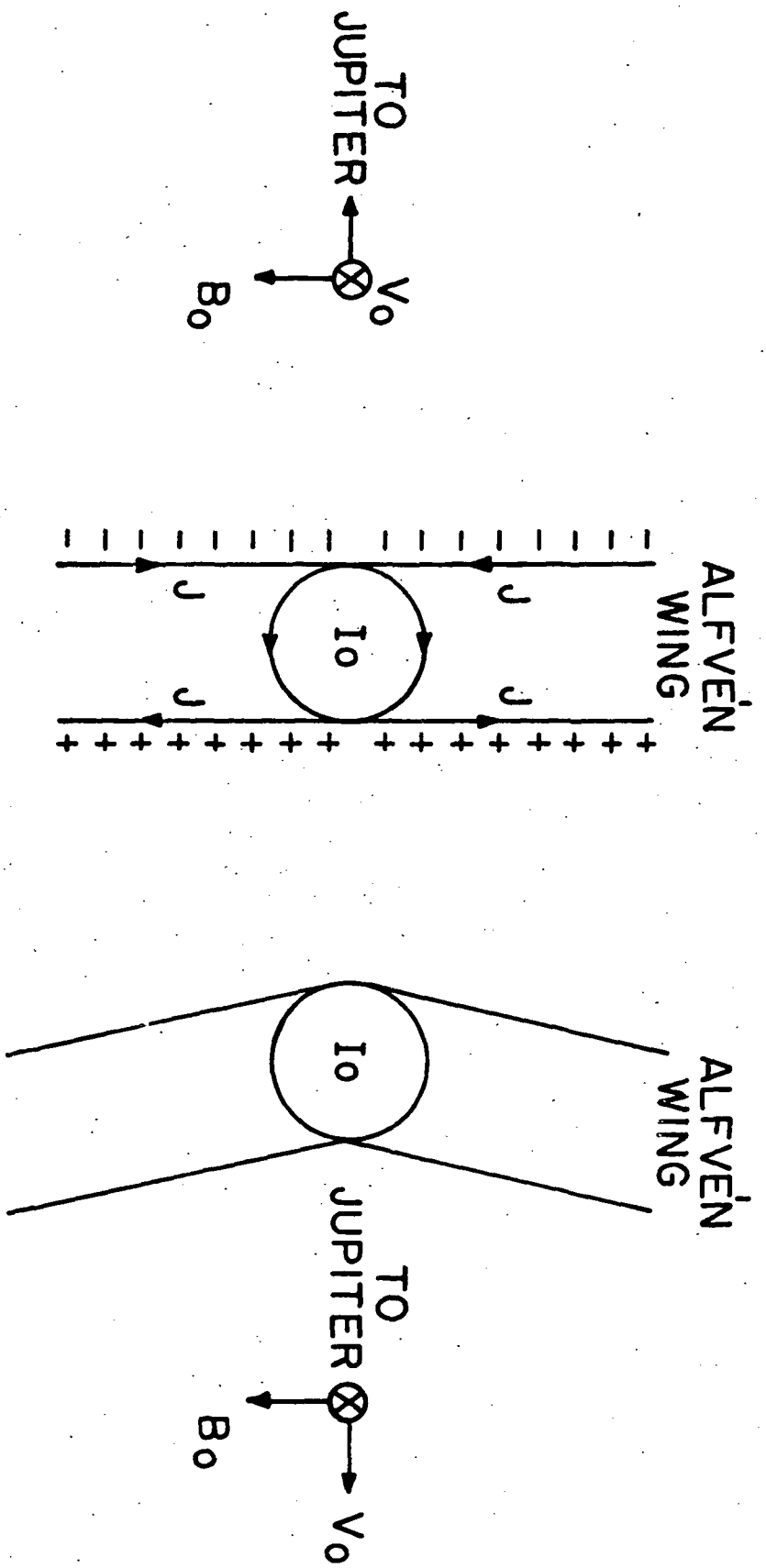
TO JUPITER
Vo
Bo
J
J
J
J
Io
ALFVÉN WING
Io
ALFVÉN WING
TO JUPITER
Bo
Vo

Figure 6

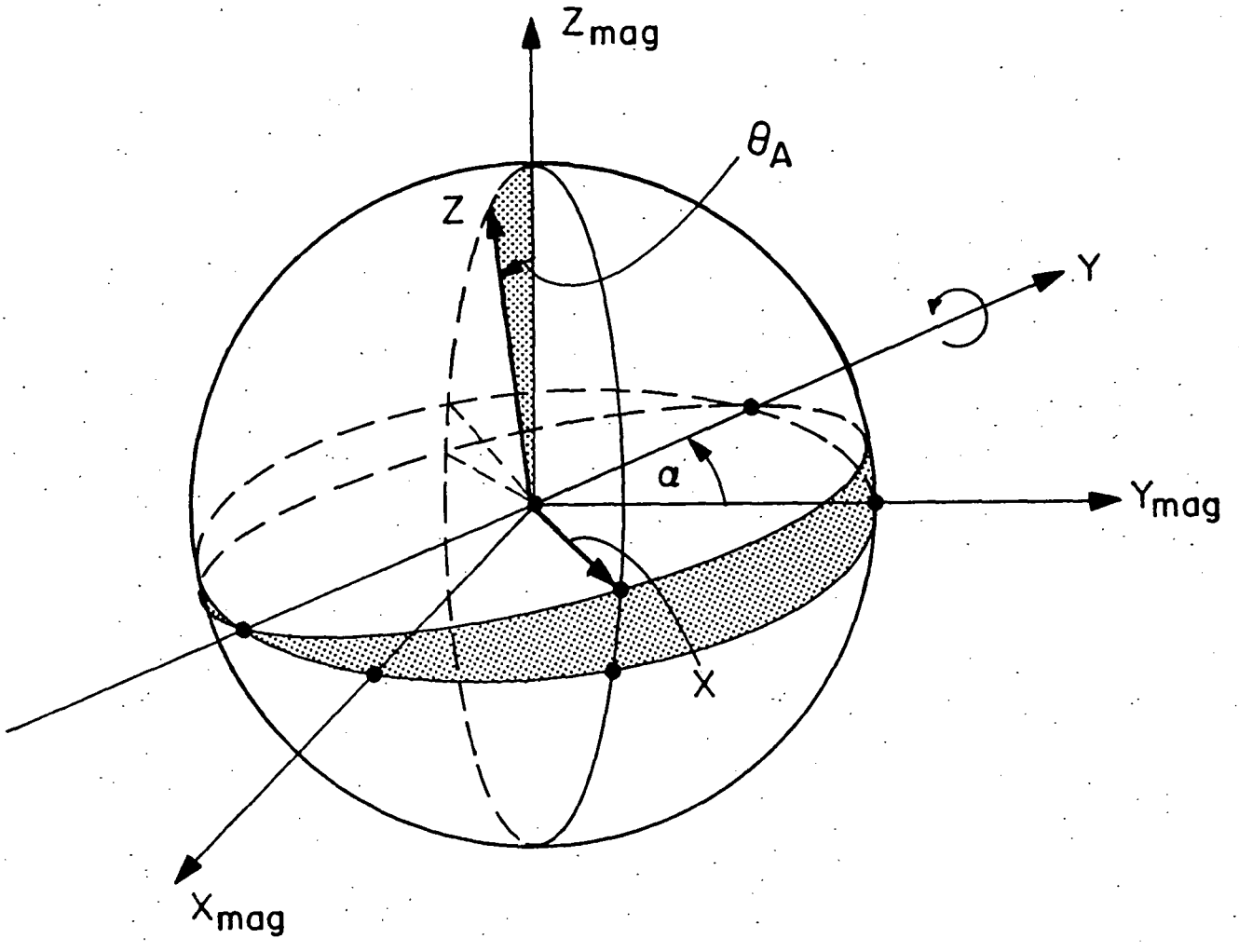

Figure 7

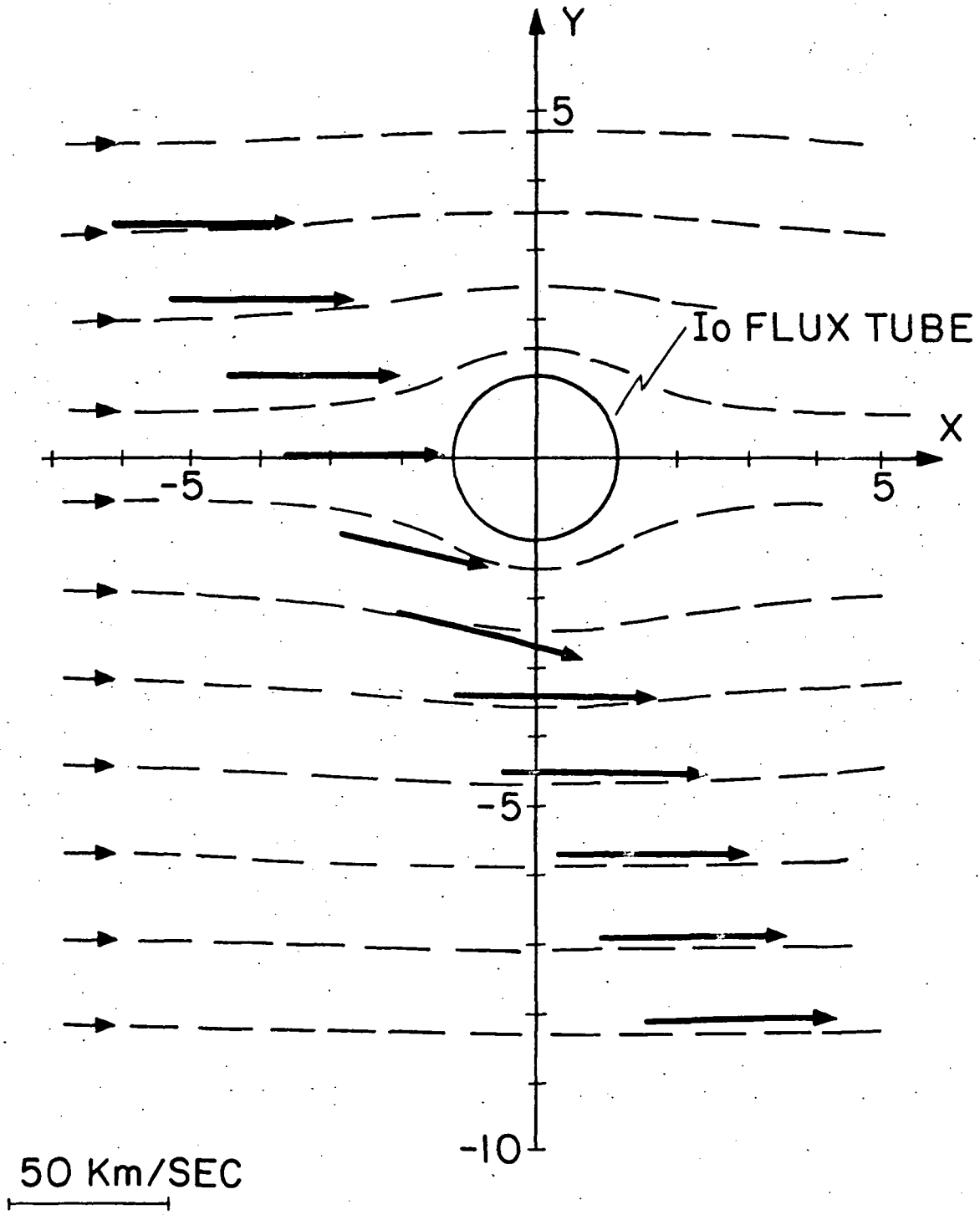

Figure 8

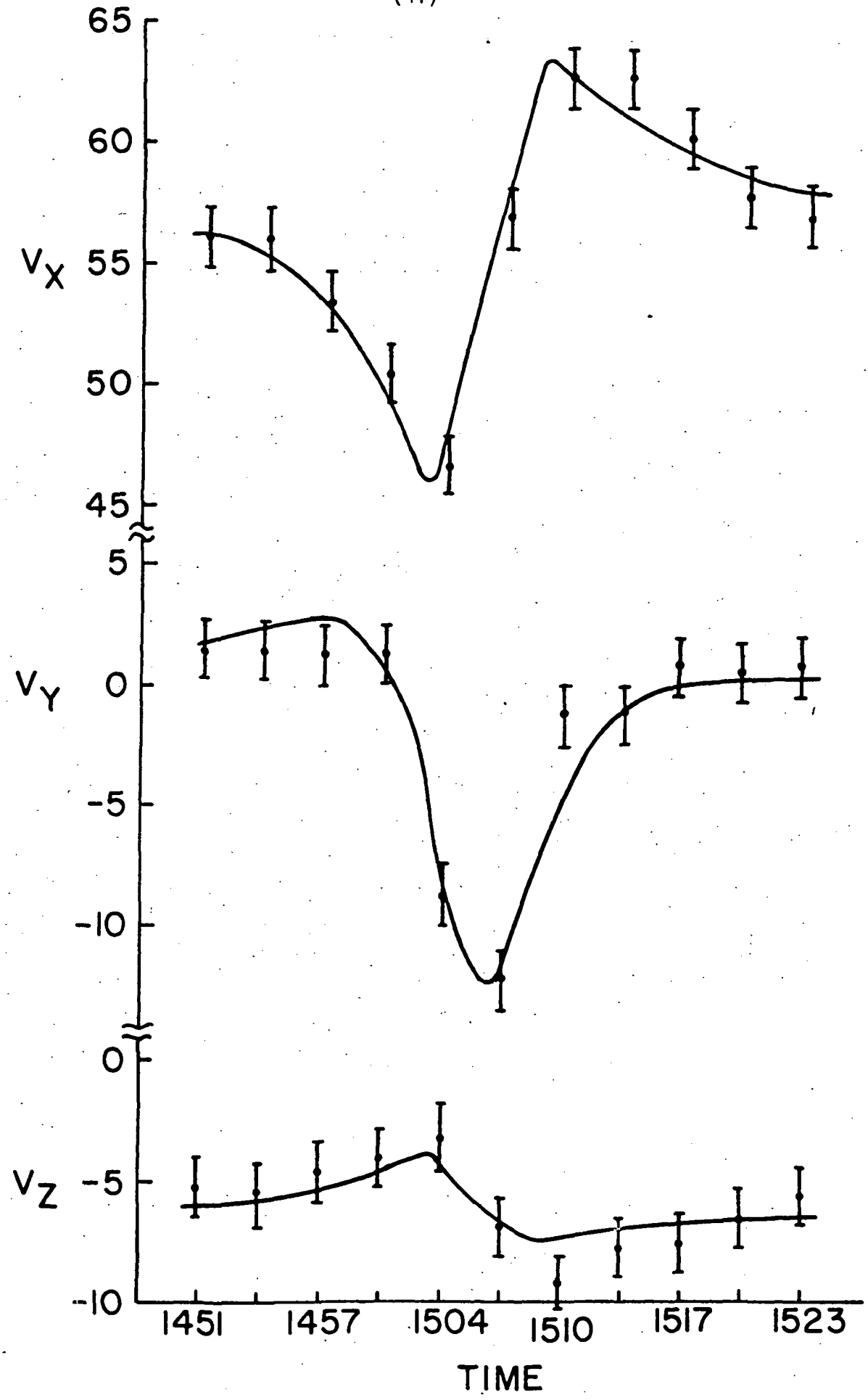
65
60
V_X 55
50
45
5
V_Y 0
-5
-10
0
V_Z -5
-10
1451
1457
1504
1510
1517
1523
TIME

Figure 9

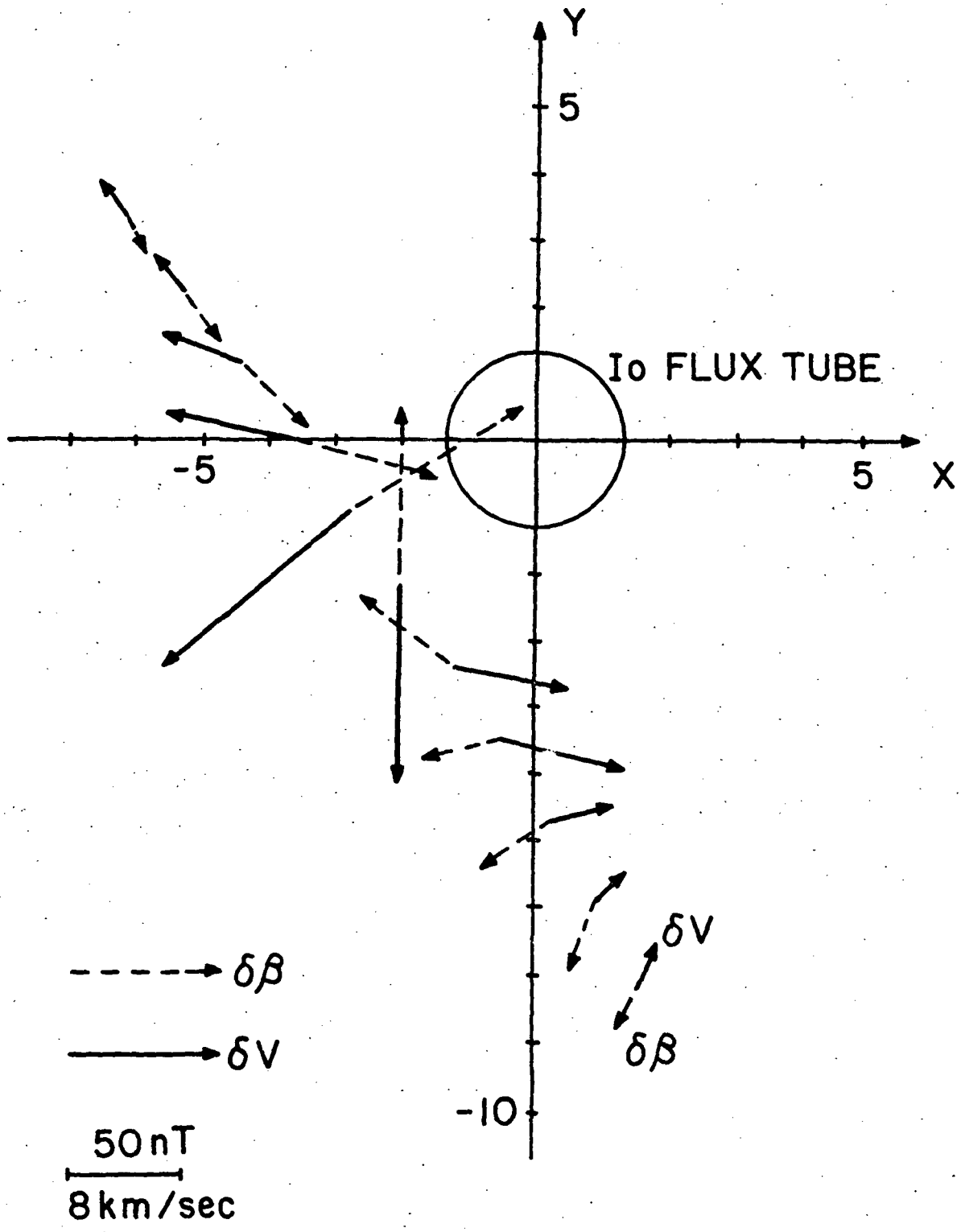

Figure 10